The Role of Electrostatics in the Interaction of the Inhibitory Region of Troponin I with Troponin C†

Darrin A. Lindhout, Robert F. Boyko, David C. Corson, Monica X. Li, and Brian D. Sykes*

CIHR Group in Protein Structure and Function, Department of Biochemistry, University of Alberta, Edmonton, Alberta, Canada T6G 2H7.

Received August 9, 2005; Revised Manuscript Received September 21, 2005

ABSTRACT: We have addressed the electrostatic interactions occurring between the inhibitory region of cardiac troponin I with the C-lobe of troponin C using scanning glycine mutagenesis of the inhibitory region. We report variations in the electric potentials due to mutation of charged residues within this complex based upon the solved NMR structure (1OZS). These results demonstrate the importance of electrostatics within this complex, and it is proposed that electrostatic interactions are integral to the formation and function of larger ternary troponin complexes. To address this hypothesis, we report ^{15}N NMR relaxation measurements, which suggest that, within a ternary complex involving the C-lobe and the N-terminal region of troponin I (residues 34−71), the inhibitory region maintains the electrostatic interactions with the E-helix of the C-lobe as observed within the binary complex. These results imply that, in solution, the cardiac troponin complex behaves in a manner consistent with that of the crystal structure of the skeletal isoform (1YTZ). A cardiac troponin complex possessing domain orientations similar to that of the skeletal isoform provides structural insights into altered troponin I activities as observed for the familial hypertrophic cardiomyopathy mutation R144G and phosphorylation of Thr142.

The contractile machinery present within the myofilament of cardiac muscle cells plays a vital role in maintaining normal heart function. The contractile proteins include myosin, actin, tropomyosin, and troponin. Troponin is a 1:1:1 complex of troponin C, troponin I, and troponin T. During diastole, troponin holds tropomyosin in a conformational state that blocks the interaction between myosin and actin (*1*−*4*). When Ca^{2+} binds to troponin C during systole, the troponin−tropomyosin complex changes so that it no longer inhibits the interaction between actin and myosin (*1*, *5*, *6*). This leads to tension producing cross-bridges between actin and myosin, potentiating actomyosin ATPase activity, and ultimately heart muscle contraction (*7*, *8*).

Cardiac troponin I (cTnI)[1] is the inhibitory component of the troponin complex, and the direct interaction with troponin C (cTnC) plays a critical role in the transmittance of the Ca^{2+} signal to myofilament proteins (*9*−*12*). Human cTnI is a 210-residue protein, differing from the skeletal isoform (sTnI) by a 33 amino acid N-terminal extension containing two serine residues (Ser22/Ser23) which are protein kinase A (PKA) substrates (*13*−*15*). cTnI is also sensitive to protein kinase C (PKC) phosphorylation at positions Ser41, Ser43, and Thr142 (*13*). The ability of cTnI to act as a target for cellular kinases represents a direct mechanism for the fine-tuning control of cardiac contraction in response to stress events and relaxation. cTnI is also functionally sensitive to mutational diseases such as familial hypertrophic cardiomyopathy (FHC), characterized by left ventricular hypertrophy, myofibril disarray, and sudden cardiac death. It is believed to be caused by mutations in cTnI (i.e., R144G, R144Q, R161W, S198N, G202S, and K205Q) and other myofibril protein components (*16*, *17*). Two of the FHC mutations and one PKC phosphorylation site are located in the critical inhibitory region (residues 128−147): a small, basic region responsible for contractile inhibition during cardiac relaxation. The inhibitory region of cTnI (cIp) has been an area of intense study with regards to specificity, binding partners, and structural coordinates, with various groups reporting conflicting results on the orientation within the troponin complex (*18*−*28*). We have previously reported the NMR solution structure of cIp bound to the C-lobe of cTnC in which the inhibitory region adopts a helical conformation with the potential for stabilizing salt-bridges between the two domains (*29*).

Recent structural studies of the troponin complex have led to a greater understanding regarding interactions among domains and their spatial orientations and resulted in proposed pathways delineating domain rearrangements occurring following a calcium initiation signal (*30*−*35*). These reports consist primarily of crystal structures and small angle neutron scattering models; however, there is little information supplied regarding the energetics of the domains within the complexes. In this study, we provide thermodynamic measurements of the interactions between key domains of the

† Supported by the Canadian Institutes of Health Research and the Heart and Stroke Foundation of Canada. D.A.L. was supported by an Alberta Heritage Foundation for Medical Research studentship.

* To whom correspondence should be addressed. Phone: (780) 492-5460. Fax: (780) 492-0886. E-mail: brian.sykes@ualberta.ca.

[1] Abbreviations: Tn, troponin; cTnI, cardiac TnI; cTnC, cardiac TnC; PKA, protein kinase A; PKC, protein kinase C; FHC, familial hypertrophic cardiomyopathy; cCTnC, C-lobe (residues 90−161) of cTnC; NMR, nuclear magnetic resonance; HSQC, heteronuclear single quantum coherence; cIp, inhibitory region of cTnI (residues 128−147); cRP40, N-terminal region of cTnI (residues 34−71); sRP40, N-terminal region of sTnI (residues 1−38).

10.1021/bi051580l CCC: $30.25
Published on Web 10/22/2005

cardiac troponin complex, with an emphasis on the inhibitory region. Using NMR, we build upon our earlier reports of the interactions of the inhibitory region of troponin I with the C-lobe of troponin C (cCTnC·cIp) using a scanning glycine mutagenesis approach (cIp, cIp-R145G, cIp-R144G, cIp-R144G-Thr142Phos, cIp-Thr142Phos), and include further mutational studies (cIp-R140G, cIp-K139G, cIp-R145G-R144G-R140G-K139G) to complete our investigation regarding the electrostatic association between these two domains (*29*, *36*−*38*). The reported binding affinities for all mutated cIp peptides with the C-lobe demonstrate a distance-dependence relationship between the two domains, such that the electric fields generated by the inhibitory region are directly influenced by mutation, and thereby affect the electrostatic environment within the binary complex. These perturbations correlate with the impairment or loss of cTnI function in heart muscle contraction. More importantly, we provide a direct relationship between the electrostatic and thermodynamic forces occurring within the binary complex cCTnC·cIp, and extend our findings to the crystal structure of the ternary skeletal troponin complex (1YTZ).

The binary complex of cCTnC·cIp was chosen for study as the use of smaller domains reduces the NMR spectral overlap and facilitates the assignment processes. However, visualization of the ternary troponin crystal structures reveals the absence of the C-lobe binding partner cRP40 ($cTnI_{34-71}$) during our mutagenesis measurements of the binary complex. To determine if the electrostatic analysis conclusions for the binary complex were valid when other C-lobe binding partners were present, we determined the ability of the inhibitory and cRP40 regions to simultaneously bind to the C-lobe using {^{1}H, ^{15}N}-HSQC NMR spectroscopy and ^{15}N NMR relaxation measurements. Solely on the basis of {^{1}H, ^{15}N}-HSQC NMR spectroscopy, it appears that cRP40 is capable of displacing the inhibitory region off the hydrophobic binding face of the C-lobe (*28*); however, ^{15}N NMR relaxation reveals that the inhibitory region remains bound to the C-lobe in the presence of cRP40. The relative lack of perturbation to C-lobe amide chemical shifts and an increase in ^{15}N-R_2 values upon cIp binding to a cCTnC·cRP40 complex suggests a ternary complex formation in which the inhibitory region is bound solely through electrostatic interactions with the C-lobe. We propose that the ternary complex of cCTnC·cRP40·cIp involves the same electrostatic interactions as we report for the cCTnC·2Ca^{2+}·cIp binary complex based upon our mutagenesis studies. These data are consistent with a cardiac isoform that behaves, in solution, in a manner similar to the domain orientations and interactions observed for the crystal structure of skeletal troponin in that the cRP40 binds across the hydrophobic face of the C-lobe with the inhibitory region making salt-bridging interactions with acidic residues predominantly on the E-helix of cTnC (*35*).

EXPERIMENTAL PROCEDURES

Sample Synthesis and Preparation. The engineering of the expression vector for the cCTnC (90−161) and expression/purification of the recombinant protein in *Escherichia coli* BL21 DE3 (pLysS) cells (^{2}H, ^{15}N, and/or ^{13}C) are as previously described (*36*, *39*, *40*). Peptides cIp, cIp-R145, cIp-R144G, cIp-T142-Phos, and cIp-R144G/T142-Phos were synthesized via standard peptide synthetic procedures, and titration against cCTnC is as previously described (*36*, *38*). Three mutant synthetic peptides of wild-type cIp were synthesized via standard peptide synthetic procedures for titration studies against cCTnC: cIp-K139G, acetyl-TQKIFDLRGKF**G**RPTLRRVR-amide; cIp-R140G, acetyl-TQKIFDLRGKFK**G**PTLRRVR-amide; and cIp-G4 (K139G, R140G, R144G, R145G), acetyl-TQKIFDLRGKF**GG**PTL**GG**VR-amide. For titration, binding, and ^{15}N-relaxation measurements of cCTnC in complex with the N-terminal cTnI domain ($cTnI_{33-71}$, cRP40), a synthetic peptide was produced via standard peptide synthetic procedures with the sequence acetyl-AKKKSKISASRKLQLKTLLLQIAKQELEREAEERRGEK-amide. Following synthesis, all synthetic peptides were lyophilized twice to remove any residual organic solvents.

Titration of ^{15}N-cCTnC·Ca^{2+} with cIp-K139G. ^{15}N-cCTnC (5.44 mg) was dissolved in 575 μL of NMR buffer (100 mM KCl, 10 mM Imdz, pH 6.7, 0.001% NaN_3, and 17 mM $CaCl_2$) and sterile-filtered and 500 μL was aliquoted into a clean 5 mm NMR tube. Solid, lyophilized cIp-K139G peptide (7.66 mg) was dissolved in 60 μL of NMR buffer and centrifuged in a 1.5 mL sterile, 0.22 μm Nylon spin-filter (Costar, Corning Incorporated) at 3000 rpm for 10 min to remove all impurities and any undissolved sample. The titration was composed of a total of 17 data points in which there were five separate additions of 1 μL of the cIp-K139G solution added directly to the NMR tube, followed by three additions of 1.5 μL, two additions of 2 μL, two additions of 3 μL, and single additions of 4, 5, 8, 10, and 15 μL, respectively. After every titration point, 1 μL of the resulting titrated solution was removed from the NMR tube and used for amino acid analysis. There was a small alkaline shift in pH during the titration, which was corrected with small amounts of 0.1 M HCl. The change in cCTnC·2Ca^{2+} concentrations due to aliquot additions during the titration was taken into account during data analysis. Both 1D ^{1}H NMR and 2D {^{1}H, ^{15}N}-HSQC spectra were acquired at every titration point.

Titration of ^{15}N-cCTnC·2Ca^{2+} with cIp-R140G. ^{15}N-cCTnC (mg) and cIp-R140G (9.57 mg) were separated, weighed out, and prepared in an identical manner to that described for the cIp-K139G titration, except that the cIp-R140G peptide was dissolved in 42 μL of NMR buffer. The titration was composed of a total of 16 data points in which there were six separate additions of 1 μL of the cIp-R140G solution added directly to the NMR tube, followed by three additions of 2 μL, two additions of 3 μL, and single additions of 5, 6, and 12 μL, respectively. After every titration point, 1 μL of the resulting titrated solution was removed from the NMR tube and used for amino acid analysis. There was a similar alkaline shift in pH during the titration as observed for cIp-K139G, which was again corrected with small amounts of 0.1 M HCl. The change in cCTnC·2Ca^{2+} concentrations due to aliquot additions during the titration was taken into account during data analysis. Both 1D ^{1}H NMR and 2D {^{1}H, ^{15}N}-HSQC spectra were acquired at every titration point. During amino acid analysis, glass tubes containing titration points 1, 2, 5, and 14 ruptured during heated acid hydrolysis and the samples were unrecoverable; therefore, for data analysis, only 12 titration points were used for calculating kinetic values.

Titration of ^{15}N-cCTnC·2Ca^{2+} with cIp-G4 (K139G, R140G, R144G, R145G). ^{15}N-cCTnC (6.75 mg) and cIp-G4 (7.35 mg) were separated, weighed out, and prepared in an identical manner to that described for the cIp-K139G titration, except that the cIp-G4 peptide was dissolved in 80 μL of NMR buffer. The titration was composed of a total of 14 data points in which there were four separate additions of 1 μL of the cIp-G4 solution added directly to the NMR tube, followed by two additions of 2 μL, and single additions of 3, 4, 5, 7, 10, 15, and 25 μL, respectively. A small amount of white precipitate was observed with increasing amounts of cIp-G4. The sample was centrifuged for 10 min at 8000 rpm to remove insoluble matter, and 1 μL of the resulting titrated solution was removed from the NMR tube for amino acid analysis for each titration point. There was a similar alkaline shift in pH during the titration as observed for cIp-K139G, which was again corrected with small amounts of 0.1 M HCl. The change in cCTnC·2Ca^{2+} concentrations due to aliquot additions during the titration was taken into account during data analysis. Both 1D ^{1}H NMR and 2D {^{1}H, ^{15}N}-HSQC spectra were acquired at every titration point.

Competition Binding Studies of cIp and cRP40 Peptides for ^{15}N-cCTnC·2Ca^{2+}. ^{15}N-cCTnC (13.88 mg) was dissolved in 1100 μL of NMR buffer (pH 6.7) and sterile-filtered, and 525 μL was separately aliquoted into two clean 5 mm NMR tubes. For the first titration series (cRP40 followed by cIp), a total of 12 titration points were acquired when solid lyophilized cRP40 peptide was added directly to one of the NMR tubes containing ^{15}N-cCTnC·2Ca^{2+} in 0.1 mg additions for the first four additions, followed by three additions of 0.25 mg, three additions of 0.5 mg, and two final additions of 1 mg to reach a saturated ^{15}N-cCTnC·2Ca^{2+}·cRP40 complex. Following the final cRP40 titration point, longitudinal and transverse ^{15}N NMR relaxation experiments were acquired. Solid, lyophilized cIp peptide (8.38 mg) was dissolved in 50 μL of NMR buffer (pH 6.7) and centrifuged in a 1.5 mL sterile, 0.22 μm Nylon spin-filter (Costar, Corning Incorporated) at 3000 rpm for 10 min to remove all impurities and any undissolved sample. To the sample tube containing ^{15}N-cCTnC·2Ca^{2+}·cRP40, a total of five titration points were acquired with additions of 2, 5, 10, 15, and 18 μL of the cIp solution to create a saturated complex of ^{15}N-cCTnC·2Ca^{2+}·cRP40·cIp. Longitudinal and transverse ^{15}N NMR relaxation experiments were acquired. Both 1D ^{1}H NMR and 2D {^{1}H, ^{15}N}-HSQC spectra were acquired at every titration point, with the pH kept constant using small additions of 0.1 M HCl when required.

For the second titration series (cIp followed by cRP40), 8.29 mg of cIp peptide was dissolved in 50 μL of NMR buffer (pH 6.7) and was prepared identically to that for the first titration series. The titration was composed of a total of 10 data points in which there were four separate additions of 1 μL of the cIp solution added directly to the other NMR tube containing ^{15}N-cCTnC·2Ca^{2+}, followed by two additions of 2 μL, and single additions of 3, 5, 10, and 24 μL, respectively, to create a saturated complex of ^{15}N-cCTnC·2Ca^{2+}·cIp. Longitudinal and transverse ^{15}N NMR relaxation experiments were acquired. A further titration of cRP40 to the ^{15}N-cCTnC·2Ca^{2+}·cIp complex was then preformed with a total of 10 data points in which solid, lyophilized cRP40 peptide was added directly to the NMR tube in 0.1 mg additions for the first three additions, followed by three additions of 0.25 mg, two additions of 0.5 mg, and two final additions of 1 mg. Longitudinal and transverse ^{15}N NMR relaxation experiments were acquired. Both 1D ^{1}H NMR and 2D {^{1}H, ^{15}N}-HSQC spectra were acquired at every titration point, with the pH kept constant using small additions of 0.1 M HCl when required.

NMR Spectroscopy. All NMR spectral data were obtained using a Unity INOVA 500 MHz spectrometer at 30 °C. 1D ^{1}H NMR spectra were acquired using a sweep width of 6000 Hz with 32 transients. 2D {^{1}H, ^{15}N}-HSQC spectra were acquired using the sensitivity-enhanced gradient pulse scheme (*41*, *42*), using ^{1}H and ^{15}N sweep widths set to 6000 and 1500 Hz with 16 transients and 128 increments. Spectral processing of all {^{1}H, ^{15}N}-HSQC was performed using the software package NMRPipe (*43*), and spectral viewing, assignments, and relaxation fit were performed using the software package NMRView (*44*). All samples were referenced directly (indirectly for ^{15}N dimension) to a 0.2 mM internal standard of 2,2-dimethyl-2-silapentane-5-sulfonate (Cambridge Isotope Laboratories). Prediction of ^{15}N-T_2 values was made using the software program HYDRONMR (*45*), with the following constants: temperature = 303 K, viscosity = 0.65 cP, 1.4 Å radius of beads in the shell (SIGMIN), effective radius of the atomic elements = 3.1 Å, $\gamma_N = -2.7126 \times 10^7$ rad·s^{-1}·T^{-1}, H−N bond length = 1.02 Å, ^{15}N chemical shift anisotropy = −160 ppm, magnetic field strength = 11.7 T. The skeletal crystal structure 1YTZ was used as a template to produce four equivalent pdb files to that of the experimental cardiac complexes (sCTnC, sCTnC·sIp, sCTnC·sRP40, and sCTnC·sIp·sRP40) (*35*).

^{15}N NMR T_1 and T_2 Relaxation Parameters. All relaxation data were acquired using an INOVA 500 MHz NMR spectrometer at 30 °C. The delay times used for ^{15}N-T_1 relaxation measurements were set to 11.1, 55.5, 122.1, 199.8, 277.5, 388.5, 499.5, 666, 888, and 1100 ms, respectively. The delay times used for ^{15}N-T_2 relaxation measurements were set to 16.61 × n ms (where n = 1, ..., 11). All other parameters were set equal to the {^{1}H, ^{15}N}-HSQC parameters previously listed.

cTnI Sequence Numbering. The numbering of the residues of cTnI in this study are as previously presented (*46*), in contrast to the numbering of the wild-type protein, which has an extra N-terminal Met residue (*47*).

RESULTS

Figure 1A indicates the location in the primary sequence of the mutations studied. The position of each mutation in relation to the structure of the inhibitory region when bound to the C-lobe of cTnC is shown in Figure 1B (*29*). The binding of cIp to the C-lobe was monitored using two-dimensional {^{1}H, ^{15}N}-HSQC NMR spectroscopy of the backbone resonances of ^{15}N-cCTnC. The NMR assignments of the C-lobe in the calcium-saturated state have been previously reported and were used as starting points to monitor protein−peptide chemical shift changes (*29*, *36*, *48*). For all peptides studied, the chemical shift perturbations were in the NMR fast exchange time scale limit yielding a linear movement of all cross-peaks, indicating that only two species (free and bound) existed in solution. Resonances undergoing large backbone amide ^{1}HN and/or ^{15}N chemical shift perturbations were measured for each peptide (*36*). Chemical

A

Peptide Name	Sequence
cIp	TQKIFDLRGKFKRPT LRRVR
cIp-K139G	TQKIFDLRGKFGRPT LRRVR
cIp-R140G	TQKIFDLRGKFKGPT LRRVR
cIp-T142Phos	TQKIFDLRGKFKRPpT LRRVR
cIp-R144G	TQKIFDLRGKFKRPT LGRVR
cIp-R144G-T142Phos	TQKIFDLRGKFKRPpT LGRVR
cIp-R145G	TQKIFDLRGKFKRPT LRGVR
cIp-G4	TQKIFDLRGKFGGPT LGGVR

B

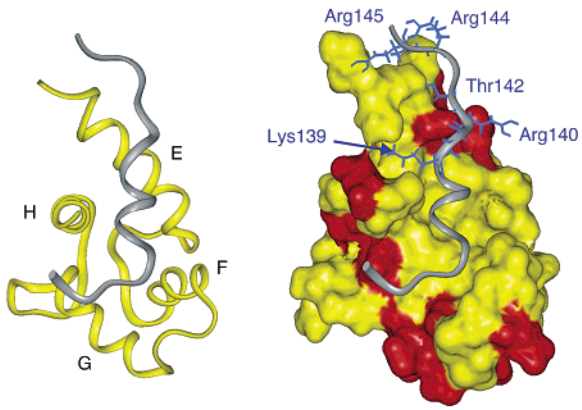

FIGURE 1: Mutagenesis of cIp peptides used to monitor the electrostatic binding effects of cIp to the C-lobe of cTnC. (A) The altered region (Lys139 to Arg145) of cIp with basic residues colored blue, threonine colored green, and hydrophobic/unaltered colored yellow. Sites of mutation(s) and phosphorylation are indicated in bold and red. The mutant peptide cIp-G4 contains four mutations (K139G, R140G, R144G, R145G). (B) Ribbon diagram of a single model from the NMR ensemble structure 1OZS. Left panel, orientation of C-lobe helices (yellow) and the inhibitory region (gray). Right panel, Connolly surface representation of the C-lobe with all acidic residues colored in red, and residues undergoing mutation/phosphorylation are indicated in blue.

shift data was fit to eq 1 to obtain a dissociation constant (K_D) and a limiting chemical shift for the titration of each individual peptide. All peptide titration curves were then re-normalized relative to one another based upon final chemical shifts to produce the binding curves displayed in Figure 2A, which correspond to additions from 0 to 8 molar equivalents of each peptide to the C-lobe. Derivation of dissociation constants were in keeping with methodology used for the wild-type peptide cIp using the software fitting program xcrvfit and are reported in Table 1 (*29*, *36*, *38*, *49*).

$$\text{cCTnC}\cdot 2\text{Ca}^{2+} + \text{cIp} \leftrightarrow \text{cCTnC}\cdot 2\text{Ca}^{2+}\cdot\text{cIp} \qquad (1)$$

A trend regarding the placement of a charged residue on the inhibitory region versus the dissociation constant can be observed. The affinity between the two domains is charge-dependent, which can be attributed to oppositely charged residues making favorable attractions between the two domains. As the mutation (i.e., $+1 \rightarrow 0$) moves from the C-terminal tail of cIp (i.e., R145G, $K_D \sim 123$ μM) toward the N-terminal region of cIp (i.e., R140G, $K_D \sim 1488$ μM), the affinity for the C-lobe diminishes. The dependence is sensitive such that the removal of arginines only five residues apart (wild-type versus R140G, R145G) causes a difference in binding affinity on the order of 1 magnitude. Upon inspection of this structure, it becomes clear how a change of a basic residue to a noncharged residue may have a strong effect, considering proximity to the acidic C-lobe. The exact position of the side chains is not known, however, as this structure contained no restraints for residues Arg140 to Arg147; thus, the C-terminal tail of cIp appears completely labile in solution (*29*). However, ^{15}N NMR relaxation data for ^{15}N-cIp in this complex revealed that cIp binds rigidly to the C-lobe except for the N- and C-terminal residues (*29*). Given the basic character of cTnI and acidic character of the C-lobe, electrostatic interactions clearly occur between the two domains. Moreover, electrostatic forces are less distance-dependent and extend their respective influences well beyond the ~5 Å NOE limit ($1/r^6$) used in NMR experiments.

Overlay of the {^{1}H, ^{15}N}-HSQC titration spectra for each individual peptide reveals that, although the peptides bind to the C-lobe with differing dissociation constants, chemical shift changes to the C-lobe remain virtually unchanged throughout the scanning mutagenesis study, suggesting that the binding site and the structure of the complex are unchanged in the mutated state (Figure 2B). Thus, the structural changes can be assumed to be the same for the binding of each peptide. This is a critical assumption of any mutagenesis approach, so that changes in the observed binding free energy can be attributed only to the residue(s) mutated/modified, and not concomitant structural changes. The absolute chemical shift change was calculated using the protocol as previously described (*36*).

To quantitate the electrostatic interactions occurring within this binary complex, the distances between the interacting side chains of the two domains were determined in the context of the ensemble of 30 reported NMR structures (1OZS), with a number of assumptions. Given that a charged particle in solution can exert an electric potential across relatively large distances (≥20 Å), we calculated the potential energy between each point mutation on the cIp peptide to all of the acidic residues within the C-lobe for all members of the ensemble. Interactions of acidic and basic cIp residues (total of nine, plus one phosphorylated Thr residue) with acidic and basic C-lobe residues (total of 32) were evaluated, including both attractive and repulsive forces. The calculations of potential energy (eq 2) follow the mutational pattern shown in Figure 3, where h is over the number of structures in the pdb ensemble, i is over the point charges on cIp, and j is over the point charges on the C-lobe. Phosphate groups were considered to have an elementary charge of -1 in the buffered solution at pH 6.7, based on the pK_a values of phosphoric acid, which are 2.15, 7.20, and 12.15, respectively.

$$E = \frac{1}{30}\sum_{h=1}^{30}\sum_{i=1}^{10}\sum_{j=1}^{32}\frac{Q_iQ_j}{4\pi\epsilon_0\epsilon r_{ij}} \qquad (2)$$

For potential energy calculations, an assumed dielectric constant (ϵ) of 80 was chosen with the permittivity of a vacuum constant (ϵ_0) of 8.854×10^{-12} C^2 J^{-1} m^{-1} and an elementary particle charge (Q) value of $\pm 1.602 \times 10^{-19}$ C. All side-chain moieties were treated as assumed point-charges, with distances derived from the carboxylate carbons for Asp/Glu residues (IUPAC nomenclature, atoms CG/CD), the amine nitrogen for Lys residues (NZ), the carbon of the guanidinyl group for the Arg residues (CZ), and the side-chain hydroxyl oxygen for Thr residues (OG1). For free-energy calculations (ΔG), a temperature value (T) of 303.15

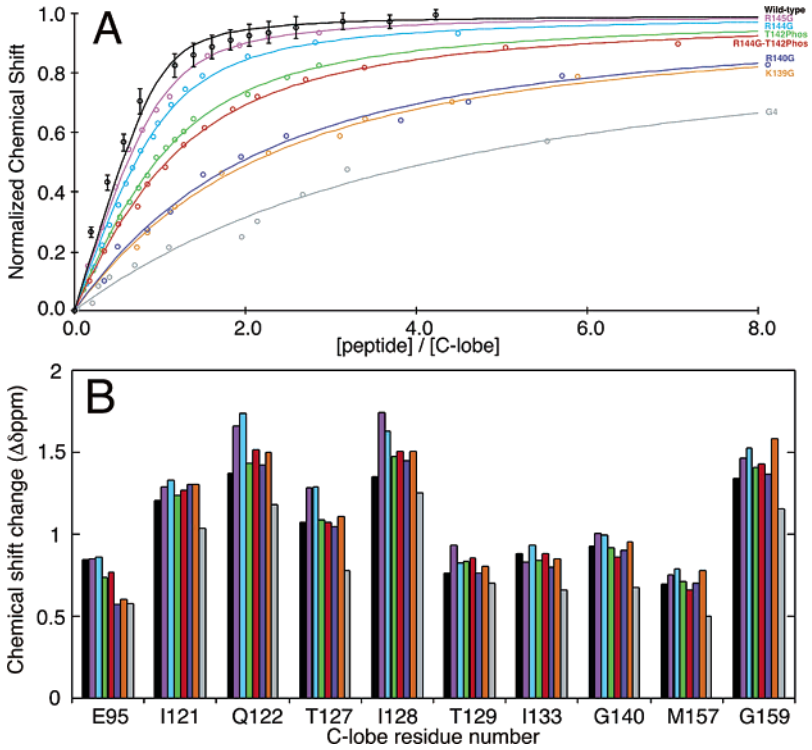

FIGURE 2: Dissociation constants and chemical shift changes for various cIp mutant peptides with the C-lobe of cTnC. (A) The binding curves for eight peptides to the C-lobe, spanning 0−8 molar additions, with experimental error displayed for the wild-type peptide. (B) Induced chemical shift changes of the C-lobe by cIp peptides. C-lobe residues indicated are those that underwent chemical shifts changes greater than one standard deviation from the average and are reported as end-point titration values.

Table 1: Dissociation Constants of Various cIp Peptides Binding to the C-Lobe of cTnC

peptide name	K_D (μM)	affinity reduction[a]
cIp -wild-type	31 ± 11	1.0
cIp-R145G	123 ± 17	4.0
cIp-R144G	193 ± 21	6.2
cIp-T142Phos	451 ± 10	14.6
cIp-R144G-T142Phos	581 ± 12	18.7
cIp-R140G	1448 ± 150	46.7
cIp-K139G	1582 ± 133	51.0
cIp-G4	3667 ± 715	118.3

[a] Calculated using the K_D values of each individual mutant peptide compared to the wild-type peptide.

K (30 °C) and a gas constant (R) of 8.315 J K^{-1} mol^{-1} were assumed (see eq 3), with K_D values obtained from analysis of {^{1}H, ^{15}N}-HSQC spectra using eq 1.

$$\Delta G = -RT \ln K_{\text{association}} = RT \ln K_{\text{Dissociation}} \quad (3)$$

The free energy component (ΔG) for any reaction can be broken up into enthalpic (ΔH) and entropic (ΔS) contributions, shown in eq 4.

$$\Delta G = \Delta H - T\Delta S \quad (4)$$

The enthalpic contribution to the free energy can be considered the summation of a potential energy term (ΔE), plus a work term, shown in eq 5.

$$\Delta H = \Delta E + \text{work} \quad (5)$$

Substitution of eq 5 into eq 4, yields eq 6. To simplify the relationship, all contributions other than the energy of

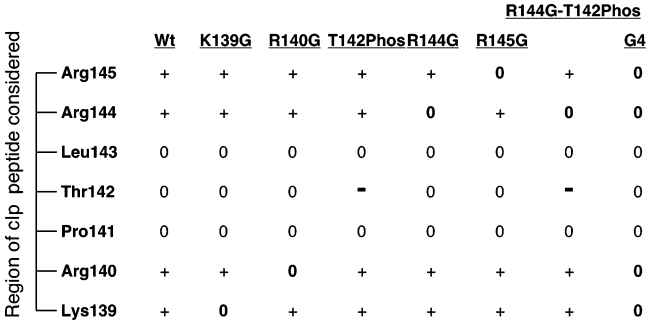

FIGURE 3: Mutational analysis of the inhibitory peptide. Schematic diagram of the placement of charges on cIp that were used in calculating the potential energy of interaction with the C-lobe. A (+) symbol indicates an elementary particle point charge of 1.602 × 10^{-19} C, a (-) symbol indicates a point charge of −1.602 × 10^{-19}, and a **0** indicates zero net charge.

interaction within the binary complex are assumed to remain constant and are represented as the term C.

$$\Delta G = \frac{1}{30}\sum_{h=1}^{30}\sum_{i=1}^{10}\sum_{j=1}^{32}\left(\frac{Q_iQ_j}{4\pi\epsilon_0\epsilon}\right)\frac{1}{r_{ij}} + C \quad (6)$$

The calculated thermodynamic values for free energy of binding and potential energy for all cIp mutations and/or phosphorylation events are listed in Table 2 and were used in the construction of Figure 4A. The plot reveals a near-linear relationship for the binding of the modified cIp peptides with the C-lobe; however, the line of best fit does not include the value for the G4 peptide. The deviation observed for this peptide is not surprising, considering the fitted binding constant (K_D = 3667 ± 715 μM) was higher than the concentration of the NMR sample tested in the

Table 2: Thermodynamic Data of cIp Peptides Binding to the C-Lobe of cTnC

peptide name	potential energy E (J/mol)[a]	free energy ΔG (J/mol)
cIp-wild-type	-73830 ± 5461	-26169
cIp-R145G	-66362 ± 5028	-22695
cIp-R144G	-65158 ± 4659	-21559
cIp-T142-Phos	-63592 ± 5172	-19420
cIp-R144G/T142-Phos	-54921 ± 4303	-18781
cIp-R140G	-61665 ± 4772	-16479
cIp-K139G	-61846 ± 5180	-16256
cIp-G4	-33482 ± 3613	-14137

[a] Derived from the average distance, taken from the 30 lowest energy calculated ensemble of the solved NMR structure 1OZS (*29*), with all charged groups treated as point charges. The error is defined as one standard deviation of the mean for all calculations.

titration, contributing to a large error, as is the case of peptides K139G ($K_D = 1448 \pm 150\ \mu$M) and R140G ($K_D = 1582 \pm 133\ \mu$M). Further, the mutation of four basic residues to Gly may have altered the side-chain placements of the other basic residues on cIp, and the entropic changes for this quadruple mutant may be much larger than the other peptides tested, all of which were single mutants with the added exception of R144G/T142-Phos. The thermodynamic value for the double mutant R144G-Thr142Phos also lies outside the curve of best fit, which, as in the case of the G4 peptide, is attributed to entropic changes. The linear relationship observed in Figure 4A implies that the major electrostatic potentials dominate other effects assumed constant in eq 6.

The electrostatic analysis performed on the ensemble of structures correlates with the measured thermodynamic data for the wild-type and mutant peptides within the binary complex. Are these interactions important in the context of the intact troponin complex? Mercier et al. have shown, for the skeletal isoform, that the binding of sRP40 displaces the inhibitory region off the C-lobe (*28*). Furthermore, the Takeda et al. X-ray crystal structure of the cardiac troponin complex shows the inhibitory region displaced off the C-lobe (*30*). However, Vinogradova et al. recently reported a crystal structure of the skeletal isoform where the inhibitory region is interacting with the C-lobe (E-helix) via electrostatic interactions (*35*), involving the same basic residues of sIp that were mutated in our cIp study. Thus, we have repeated the calculations for the electrostatic potentials based upon the distances observed within the skeletal crystal structure 1YTZ, and plotted them against our reported free-energy values for the cardiac isoform. The resultant plot shown in Figure 4B is remarkably similar to that reported for the cardiac binary complex. Absent from the skeletal plot are reported values involving Thr110, as this is a Pro residue in the wild-type skeletal sequence. We could not perform the equivalent calculation for the cardiac crystal structure (1J1D or 1J1E), as there was a lack of electron density reported for the inhibitory region (*30*).

The results reported above suggest that the electrostatic interaction between cIp and the C-lobe is present in the troponin complex. We have therefore investigated the relative binding of the cIp and cRP40 to the C-lobe. $\{^1H, ^{15}N\}$-HSQC NMR spectra show that the C-lobe is capable of binding either cIp or cRP40 separately through the observation of C-lobe chemical shift changes upon binding (data not shown). However, the addition of cRP40 to the binary complex of

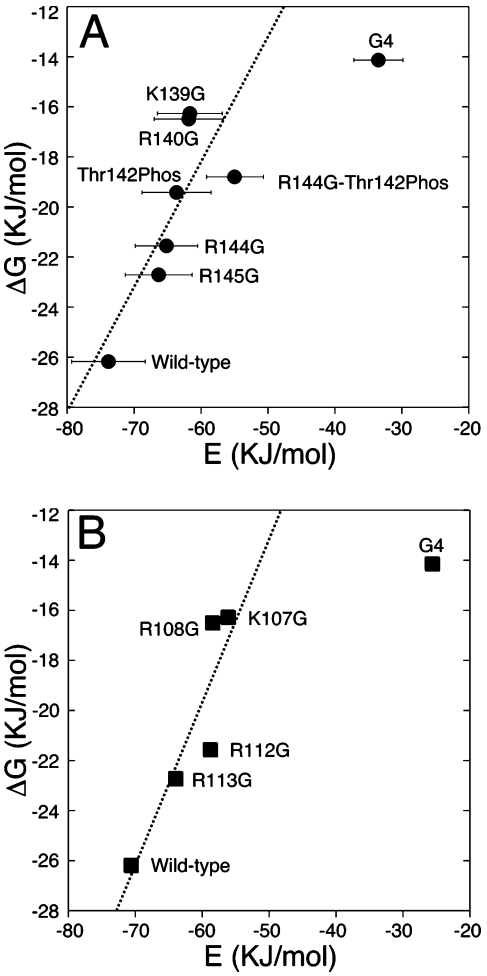

FIGURE 4: Relationship of free energy of binding (ΔG) versus potential energy (E). Thermodynamic values generated from scanning glycine mutagenesis/phosphorylation of cardiac cIp peptides compared to the calculated potential energy values for (A) the NMR ensemble 1OZS and (B) the crystal structure of the skeletal troponin complex 1YTZ. A line of best fit is shown for all data (excluding G4). All potential energy values are negative, which implies an attractive electrostatic force between the domains.

cCTnC·$2Ca^{2+}$·cIp yields $\{^1H, ^{15}N\}$-NMR chemical shifts almost identical to those of just the cCTnC·$2Ca^{2+}$·cRP40 complex. This result suggests that cIp is being displaced from the C-lobe by cRP40 via a competitive binding mechanism. This was confirmed by the observation that the addition of cIp to a cCTnC·$2Ca^{2+}$·cRP40 binary complex resulted in only a minor perturbation of the amide chemical shifts. These results mirror those reported by Mercier et al. who concluded that the inhibitory region cannot bind the skeletal C-lobe in the presence of sRP40 (*28*). To test whether cRP40 actually displaces cIp from the C-lobe, we acquired ^{15}N NMR relaxation data at 500 MHz for ^{15}N-cCTnC·$2Ca^{2+}$ alone, and in the presence of cIp, cRP40, and of both cIp and cRP40 (Figure 5A,B). The ternary complex of ^{15}N-cCTnC·$2Ca^{2+}$·cRP40·cIp had higher average ^{15}N-T_1 and lower average ^{15}N-T_2 values than that for the ^{15}N-cCTnC·$2Ca^{2+}$·cRP40 complex, indicating an increased correlation time consistent with cIp and cRP40 binding simultaneously to the C-lobe. Further additions of either cIp and/or cRP40 to the ^{15}N-cCTnC·$2Ca^{2+}$·cRP40·cIp complex did not change relaxation values, indicating that the complex is present in a 1:1:1 ratio of C-lobe·cRP40·cIp, and that there is no nonspecific binding

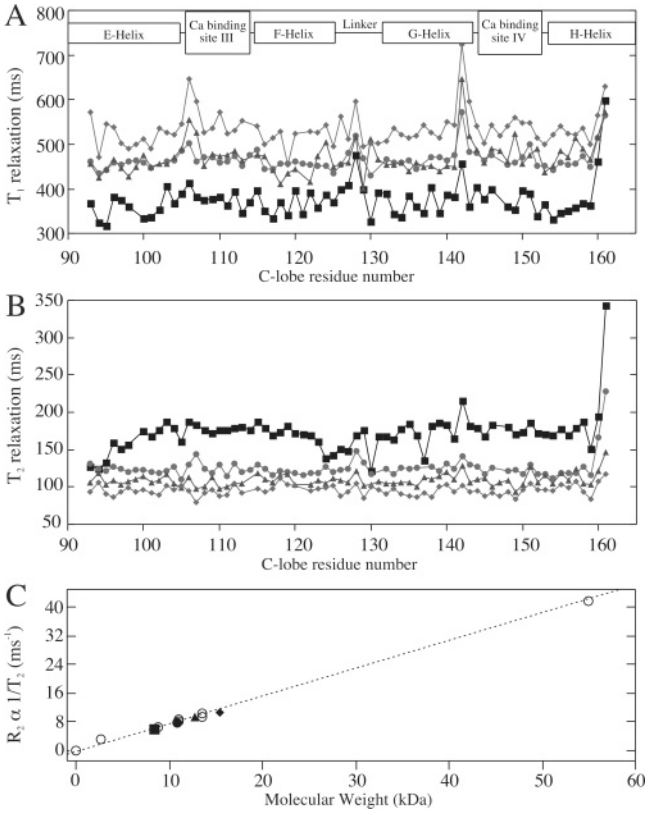

FIGURE 5: ^{15}N NMR backbone relaxation of the C-lobe of cTnC in complex with cTnI peptides. The secondary structural elements of the C-lobe backbone are diagramed above the T_1 values. (A) T_1 and (B) T_2 values are defined as follows: ■, cCTnC; ●, cCTnC·cIp; ▲, cCTnC·cRP40; and ◆, cCTnC·cRP40·cIp, as measured at 500 MHz. (C) Linear relationship of R_2 versus molecular weight for the four complexes observed in (B), compared with other troponin complexes under similar experimental conditions (○, ^{15}N-cIp (500 MHz), ^{15}N-sCTnC (500 MHz), ^{15}N-cIp·cCTnC (500/600 MHz), ^{15}N-sCTnC·sRP40 (500/600 MHz), ^{15}N-sTnC·sTnI·sTnT-T2 (800 MHz)).

of either peptide to the C-lobe. This result refutes the conclusion based upon {^{1}H, ^{15}N}-HSQC binding studies, which rely solely on chemical shift changes, and demonstrates that the cardiac C-lobe is capable of simultaneous binding of both cIp and cRP40 domains. A plot of measured ^{15}N-R_2 values for the four complexes versus molecular weight clearly demonstrates a linear relationship for the globular troponin complexes (Figure 5C). This is predicted by eq 7, where R_2 relaxation of the HN vector can be approximated (assuming the condition $\omega^2\tau_c^2 \gg 1$ for slow molecular motion) to a constant term C (involving chemical shift anisotropy and dipole−dipole effects), order parameter S^2 (model-free analysis), and a rotational correlation τ_{rot} term. The τ_{rot} term is defined in eq 8, where it is dependent on the volume for a tumbling body in solution (a, radius; η, viscosity; k, Boltzman constant; and T, temperature), in which the volume is an approximation for overall molecular weight (assuming isotropic tumbling in solution). The addition of

$$R_2 \approx CS^2\tau_{rot} \tag{7}$$

$$\tau_{rot} = \left(\frac{4\pi a^3}{3}\right)\frac{\eta}{kT} \tag{8}$$

other previously reported values for troponin complexes reveals average R_2 values that fit the linear relationship demonstrated in Figure 5C (*29*, *50*, *51*).

These results validate our reported NMR solution structure of the binary complex (1OZS), indicating that important interactions occurring between the inhibitory region and the C-lobe are predominantly electrostatic in nature and remain in the troponin complex. Additionally, they suggest that other troponin-binding partners need not be present to form a functional physiological complex between the inhibitory region and the C-lobe in solution.

DISCUSSION

The focus of this study was to verify the position of the inhibitory region with respect to the C-lobe of cTnC using a combination of electrostatic and ^{15}N NMR relaxation measurements and to correlate changes in charge arising from mutagenesis/phosphorylation with affinities, in the context of the NMR solution structure (*29*). We have previously shown that the binding of the inhibitory region to the C-lobe is mediated via a limited number of hydrophobic contacts and a significant number of electrostatic interactions (*29*, *36*, *38*). All mutations involved a change to a less positively charged inhibitory region interacting with an acidic C-lobe. The binding affinities for the peptides (see Table 1) behaved in a manner previously predicted (*29*, *52*). As the mutation gets closer in space to the C-lobe, the binding affinity becomes weaker (*36*). Two of the peptides (Thr142Phos and R144G) are known to occur in vivo and can alter muscular interactions within the sarcomere. The mutation cIp-R144G is of medical importance as it is a known cause of FHC, a disease which causes a thickening of the left ventricle of the heart resulting in premature death due to myocardial infarction in humans (*16*, *17*). Modification of Thr142 via phosphorylation by PKC primarily acts to decrease cardiac contractility by decreasing actomyosin ATPase activity.

The choice to mutate basic residues to glycine was in keeping with the biological FHC mutant R144G. Clearly, the removal of the positive charge on the Arg/Lys side chains by mutation to glycine results in the loss of the hydrophobic methylene side-chain carbon groups (i.e., -CH_2-CH_2-CH_2-CH_2-), which may affect side-chain packing required for proper complex formation. However, no hydrophobic interdomain NOEs were observed from any of the mutated side-chain cIp residues to the C-lobe in the published structure. Glycine also increases the potential for flexibility in the complex. In particular, the quadruple glycine mutant cIp-G4 might be expected to be quite flexible to the extent that the measured changes fall outside of the experimental error observed in Figure 4A. Regardless, this work clearly demonstrates the importance of charge potentials and distances within the binary complex cCTnC·cIp, and may be extended to the troponin complex as a whole.

Inspection of the skeletal and cardiac crystal structures of the troponin complex reveals different features such as TnC domain orientation (*30*, *35*). For the purpose of this study, none is more important than the positioning of the inhibitory region. The 46 and 52 kDa cardiac crystal structures lacked electron density for the cIp domain and infer that it was extended and positioned away from the C-lobe of TnC (*30*). This result is in conflict with our binary NMR structure of the inhibitory region with the C-lobe, as we reported contact

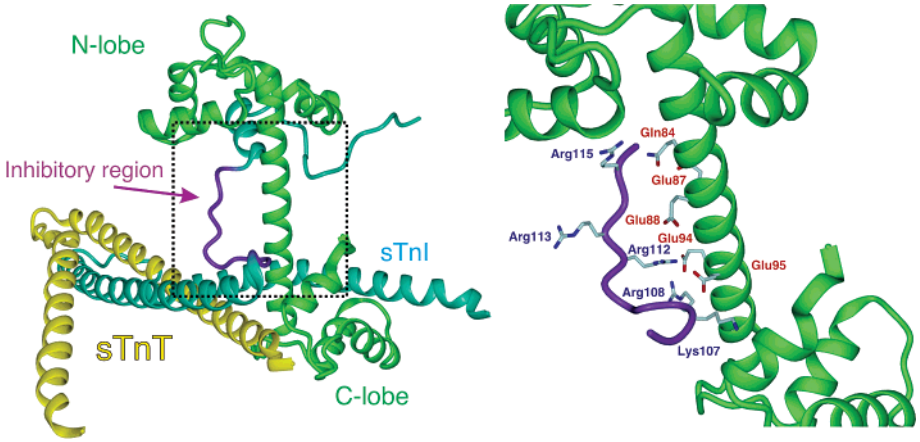

FIGURE 6: Crystal structure of the skeletal troponin complex. The skeletal crystal structure 1YTZ is displayed to the left as a ribbon diagram, with sTnC in green, sTnT in yellow, and sTnI in cyan, and the inhibitory region in purple (*35*). An expanded view of residues involved in electrostatic interactions is shown to the right. Numbering of residues is for the skeletal troponin proteins.

between the two domains (*29*). The skeletal crystal structure more closely corresponds to the NMR structure, in that the inhibitory region interacts with the E-helix of the C-lobe in the presence of sRP40 (*35*, *53*), as shown in Figure 6.

To test the ability of the C-lobe to bind cIp in the presence of cRP40, we repeated the titration experiments reported by Mercier et al. using the cardiac proteins (*28*), and included ^{15}N-T_1 and ^{15}N-T_2 relaxation data to probe the binding of the two peptides to the C-lobe. On the basis of C-lobe {^{1}H, ^{15}N}-HSQC chemical shift changes only, our results mirror those of Mercier et al. for the skeletal isoform, suggesting that the C-lobe is unable to bind cIp in the presence of cRP40. ^{15}N NMR relaxation data, however, demonstrates that the T_1 and T_2 values for the cCTnC·cRP40·cIp complex are different than those for cCTnC·cRP40 and the cCTnC·cIp complexes alone, in a manner consistent with the formation of the ternary complex. These data reveal that the inhibitory and cRP40 regions of cTnI are capable of simultaneous binding to the C-lobe. The observation that the addition of cIp to the cCTnC·cRP40 complex induced minimal {^{1}H, ^{15}N}-NMR chemical shift perturbations to the C-lobe is significant in the context of the relaxation data and the previous electrostatic binding results for cIp. The sensitivity of the {^{1}H, ^{15}N}-HSQC backbone amide chemical shifts to the chemical environment reveals that cIp binding to the C-lobe in the presence of cRP40 is not near the hydrophobic cleft of the C-lobe. More likely the salt-bridging electrostatic interactions of the side chains anchoring the cIp region onto the cCTnC·cRP40 complex have a nonperturbing effect on the C-lobe amide chemical shift values.

The linear relationship of transverse relaxation rate and molecular weight observed in Figure 5C clearly demonstrates that the ternary complex cCTnC·cIp·cRP40 forms a 1:1:1 ratio. This is as would be expected based upon the skeletal crystal structure (1YTZ), where the inhibitory region flanks the C-lobe making electrostatic interactions with the cluster of glutamate residues on the E-helix and the RP40 region bound on the hydrophobic face of the C-lobe. The reported average ^{15}N-R_2 values for the four cardiac complexes were examined against the predicted values generated using the software program HYDRONMR (*45*), as described in Experimental Procedures. The experimental relaxation rates for the cardiac complexes are within the error limits for the calculated skeletal values at a magnetic field strength of 500 MHz (sCTnC, 6.05 ± 0.27 ms^{-1}; sCTnC·sIp, 8.24 ± 0.44 ms^{-1}; sCTnC·sRP40, 8.99 ± 0.41 ms^{-1}; and sCTnC·sIp·sRP40, 11.82 ± 0.39 ms^{-1}). The fact that the relaxation values predicted using the skeletal X-ray structure mirror the experimental values obtained for the cardiac complex strongly implies that the two complexes display domain orientations in solution more closely resembling the skeletal crystal structure (*30*, *35*).

Functional implications can thus be addressed in the context of the skeletal structure 1YTZ (see Figure 6). In this structure, the inferred positioning of cardiac residue Thr142 would be easily accessible for phosphorylation by PKC. Our work establishes that a phosphorylation event in this region of the inhibitory region would be sufficient to impart an electrostatic imbalance, demonstrating a regulatory mechanism for cardiac rhythmic control. The salt-bridge observed for Arg112 of sTnI with Glu94 of sTnC would correspond to the known FHC mutation R144G in cardiac tissues. It is possible that the loss of this critical salt-bridge is sufficient to negatively alter the delicate electrostatic balance in this region of cTnI, leading to the presentation of an enlarged left ventricle within the heart. Additionally, we propose that the phosphorylation of Thr142 is an important effector of the R144G mutation, as the loss of an Arg residue at position 144 in the cardiac TnI sequencing is sufficient to abolish the phosphorylation consensus sequence (S/T-X-R/K) by PKC on Thr142.

ACKNOWLEDGMENT

We would like to thank Jeff DeVries, for spectrometer maintenance and servicing, and Angela Thiessen and Melissa Rakovszky, for protein expression and purification.

REFERENCES

1. Perry, S. V. (1999) Troponin I: inhibitor or facilitator, *Mol. Cell. Biochem. 190*, 9−32.
2. Perry, S. V. (2003) What is the role of tropomyosin in the regulation of muscle contraction?. *J. Muscle Res. Cell Motil. 24*, 593−596.
3. Tobacman, L. S. (1996) Thin filament-mediated regulation of cardiac contraction, *Annu. Rev. Physiol. 58*, 447−481.
4. Farah, C. S., and Reinach, F. C. (1995) The troponin complex and regulation of muscle contraction, *FASEB J. 9*, 755−767.
5. Filatov, V. L., Katrukha, A. G., Bulargina, T. V., and Gusev, N. B. (1999) Troponin: structure, properties, and mechanism of functioning, *Biochemistry (Moscow, Russ. Ed.) 64*, 969−985.

6. Solaro, R. J., el-Saleh, S. C., and Kentish, J. C. (1989) Ca2+, pH and the regulation of cardiac myofilament force and ATPase activity. *Mol. Cell. Biochem. 89*, 163−167.
7. Geeves, M. A., and Holmes, K. C. (1999) Structural mechanism of muscle contraction. *Annu. Rev. Biochem. 68*, 687−728.
8. Gordon, A. M., Homsher, E., and Regnier, M. (2000) Regulation of contraction in striated muscle. *Physiol. Rev. 80*, 853−924.
9. Talbot, J. A., and Hodges, R. S. (1979) Synthesis and biological activity of an icosapeptide analog of the actomyosin ATPase inhibitory region of troponin I. *J. Biol. Chem. 254*, 3720−3723.
10. Talbot, J. A., and Hodges, R. S. (1981) Synthetic studies of the inhibitory region of rabbit skeletal troponin I, *J. Biol. Chem. 256*, 2798−2802.
11. Solaro, R. J. (2003) The special structure and function of troponin I in regulation of cardiac contraction and relaxation, *Adv. Exp. Med. Biol. 538*, 389−402.
12. Solaro, R. J. (1999) Troponin I, stunning, hypertrophy, and failure of the heart, *Circ. Res. 84*, 122−124.
13. Solaro, R. J., and Rarick, H. M. (1998) Troponin and tropomyosin: proteins that switch on and tune in the activity of cardiac myofilaments, *Circ. Res. 83*, 471−480.
14. Finley, N., Abbott, M. B., Abusamhadneh, E., Gaponenko, V., Dong, W., Gasmi-Seabrook, G., Howarth, J. W., Rance, M., Solaro, R. J., Cheung, H. C., and Rosevear, P. R. (1999) NMR analysis of cardiac troponin C-troponin I complexes: effects of phosphorylation, *FEBS Lett. 453*, 107−112.
15. Gaponenko, V., Abusamhadneh, E., Abbott, M. B., Finley, N., Gasmi-Seabrook, G., Solaro, R. J., Rance, M., and Rosevear, P. R. (1999) Effects of troponin I phosphorylation on conformational exchange in the regulatory domain of cardiac troponin C, *J. Biol. Chem. 274*, 16681−16684.
16. Redwood, C. S., Moolman-Smook, J. C., and Watkins, H. (1999) Properties of mutant contractile proteins that cause hypertrophic cardiomyopathy, *Cardiovasc. Res. 44*, 20−36.
17. Hernandez, O. M., Housmans, P. R., and Potter, J. D. (2001) Invited review: pathophysiology of cardiac muscle contraction and relaxation as a result of alterations in thin filament regulation, *J. Appl. Physiol. 90*, 1125−1136.
18. Li, M. X., Spyracopoulos, L., Beier, N., Putkey, J. A., and Sykes, B. D. (2000) Interaction of cardiac troponin C with Ca2+ sensitizer EMD 57033 and cardiac troponin I inhibitory peptide, *Biochemistry 39*, 8782−8790.
19. Ngai, S.-M., and Hodges, R. S. (1992) Biologically important interactions between synthetic peptides of the N-terminal region of troponin I and troponin C, *J. Biol. Chem. 267*, 15715−15720.
20. Tripet, B., Van Eyk, J. E., and Hodges, R. S. (1997) Mapping of a second actin-tropomyosin and a second troponin C binding site within the C terminus of troponin I, and their importance in the Ca^{2+}-dependent regulation of muscle contraction, *J. Mol. Biol. 271*, 728−750.
21. Campbell, A. P., and Sykes, B. D. (1991) Interaction of troponin I and troponin C. Use of the two-dimensional nuclear magnetic resonance transferred nuclear Overhauser effect to determine the structure of the inhibitory troponin I peptide when bound to skeletal troponin C, *J. Mol. Biol. 222*, 405−421.
22. Campbell, A. P., Van Eyk, J. E., Hodges, R. S., and Sykes, B. D. (1992) Interaction of troponin I and troponin C: use of the two-dimensional transferred nuclear Overhauser effect to determine the structure of a Gly-110 inhibitory troponin I peptide analog when bound to cardiac troponin C, *Biochim. Biophys. Acta 1160*, 35−54.
23. Ngai, S.-M., Sönnichsen, F. D., and Hodges, R. S. (1994) Photochemical cross-linking between native rabbit skeletal troponin C and benzoylbenzoyl-troponin I inhibitory peptide, resideues 104−115, *J. Biol. Chem. 269*, 2165−2172.
24. Vassylyev, D. G., Takeda, S., Wakatsuki, S., Maeda, K., and Maeda, Y. (1998) Crystal structure of troponin C in complex with troponin I fragment at 2.3-Å resolution, *Proc. Natl. Acad. Sci. U.S.A. 95*, 4847−4852.
25. Hernandez, G., Blumenthal, D. K., Kennedy, M. A., Unkefer, C. J., and Trewhella, J. (1999) Troponin I inhibitory peptide (96−115) has an extended conformation when bound to skeletal muscle troponin C, *Biochemistry 38*, 6911−6917.
26. Tung, C. S., Wall, M. E., Gallagher, S. C., and Trewhella, J. (2000) A model of troponin-I in complex with troponin-C using hybrid experimental data: the inhibitory region is a beta-hairpin, *Protein Sci. 9*, 1312−1326.
27. Brown, L. J., Sale, K. L., Hills, R., Rouviere, C., Song, L., Zhang, X., and Fajer, P. G. (2002) Structure of the inhibitory region of troponin by site directed spin labeling electron paramagnetic resonance, *Proc. Natl. Acad. Sci. U.S.A. 99*, 12765−12770.
28. Mercier, P., Li, M. X., and Sykes, B. D. (2000) Role of the structural domain of troponin C in muscle regulation: NMR studies of Ca^{2+} binding and subsequent interactions with regions 1−40 and 96−115 of troponin I, *Biochemistry 39*, 2902−2911.
29. Lindhout, D. A., and Sykes, B. D. (2003) Structure and dynamics of the C-domain of human cardiac troponin C in complex with the inhibitory region of human cardiac troponin I, *J. Biol. Chem. 278*, 27024−27034.
30. Takeda, S., Yamashita, A., Maeda, K., and Maeda, Y. (2003) Structure of the core domain of human cardiac troponin in the Ca(2+)-saturated form, *Nature 424*, 35−41.
31. Heller, W. T., Abusamhadneh, E., Finley, N., Rosevear, P. R., and Trewhella, J. (2002) The solution structure of a cardiac troponin C−troponin I−troponin T complex shows a somewhat compact troponin C interacting with an extended troponin I−troponin T component *Biochemistry 41*, 15654−15663.
32. Heller, W. T., Finley, N. L., Dong, W. J., Timmins, P., Cheung, H. C., Rosevear, P. R., and Trewhella, J. (2003) Small-angle neutron scattering with contrast variation reveals spatial relationships between the three subunits in the ternary cardiac troponin complex and the effects of troponin I phosphorylation, *Biochemistry 42*, 7790−7800.
33. Matsumoto, F., Makino, K., Maeda, K., Patzelt, H., Maeda, Y., and Fujiwara, S. (2004) Conformational changes of troponin C within the thin filaments detected by neutron scattering, *J. Mol. Biol. 342*, 1209−1221.
34. King, W. A., Stone, D. B., Timmins, P. A., Narayanan, T., von Brasch, A. A., Mendelson, R. A., and Curmi, P. M. (2005) Solution structure of the chicken skeletal muscle troponin complex via small-angle neutron and X-ray scattering, *J. Mol. Biol. 345*, 797−815.
35. Vinogradova, M. V., Stone, D. B., Malanina, G. G., Karatzaferi, C., Cooke, R., Mendelson, R. A., and Fletterick, R. J. (2005) Ca^{2+}-regulated structural changes in troponin, *Proc. Natl. Acad. Sci. U.S.A. 102*, 5038−5043.
36. Lindhout, D. A., Li, M. X., Schieve, D., and Sykes, B. D. (2002) Effects of T142 phosphorylation and mutation R145G on the interaction of the inhibitory region of human cardiac troponin I with the C-domain of human cardiac troponin C, *Biochemistry 41*, 7267−7274.
37. Lindhout, D. A., Thiessen, A., Schieve, D., and Sykes, B. D. (2003) High-yield expression of isotopically labeled peptides for use in NMR studies, *Protein Sci. 12*, 1786−1791.
38. Li, M. X., Wang, X., Lindhout, D. A., Buscemi, N., Van Eyk, J. E., and Sykes, B. D. (2003) Phosphorylation and mutation of human cardiac troponin I deferentially destabilize the interaction of the functional regions of troponin I with troponin C, *Biochemistry 42*, 14460−14468.
39. Chandra, M., Dong, W. J., Pan, B. S., Cheung, H. C., and Solaro, R. J. (1997) Effects of protein kinase A phosphorylation on signaling between cardiac troponin I and the N-terminal domain of cardiac troponin C, *Biochemistry 36*, 13305−13311.
40. Li, M. X., Gagné, S. M., Tsuda, S., Kay, C. M., Smillie, L. B., and Sykes, B. D. (1995) Calcium binding to the regulatory N-domain of skeletal muscle troponin C occurs in a stepwise manner, *Biochemistry 34*, 8330−8340.
41. Kay, L. E., Keifer, P., and Saarinen, T. (1992) Pure absorption gradient enhanced heteronuclear single quantum correlation spectroscopy with improved sensitivity, *J. Am. Chem. Soc. 114*, 10663−10665.
42. Zhang, O., Kay, L. E., Olivier, J. P., and Forman-Kay, J. D. (1994) Backbone ^{1}H and ^{15}N resonance assignments of the N-terminal SH3 domain of drk in folded and unfolded states using enhanced-sensitivity pulsed field gradient NMR techniques, *J. Biomol. NMR 4*, 845−858.
43. Delaglio, F., Grzesiek, S., Vuister, G. W., Zhu, G., Pfeifer, J., and Bax, A. (1995) NMRPipe: a multidimensional spectral processing system based on UNIX pipes, *J. Biomol. NMR 6*, 277−293.
44. Johnson, B. A., and Blevins, R. A. (1994) NMRView: a computer program for the visualization and analysis of NMR data, *J. Biomol. NMR 4*, 603−614.
45. de la Torre, J. G., Huertas, M. L., and Carrasco, B. (2000) HYDRONMR: prediction of NMR relaxation of globular proteins from atomic-level structures and hydrodynamic calculations, *J. Magn. Res. 147*, 138−146.

46. Dargis, R., Pearlstone, J. R., Barrette-Ng, I., Edwards, H., and Smillie, L. B. (2002) Single mutation (A162H) in human cardiac troponin I corrects acid pH sensitivity of Ca^{2+}-regulated actomyosin S1 ATPase, *J. Biol. Chem. 277*, 34662−34665.
47. Vallins, W. J., Brand, N. J., Dabhade, N., Butler-Browne, G., Yacoub, M. H., and Barton, P. J. (1990) Molecular cloning of human cardiac troponin I using polymerase chain reaction, *FEBS Lett. 270*, 57−61.
48. Sia, S. K., Li, M. X., Spyracopoulos, L., Gagné, S. M., Liu, W., Putkey, J. A., and Sykes, B. D. (1997) Structure of cardiac muscle Troponin C unexpectedly reveals a closed regulatory domain, *J. Biol. Chem. 272*, 18216−18221.
49. Boyko, R., and Sykes, B. D. (2003) XCRVFIT: binding curve studies and curve fitting for NMR spectroscopic analysis, XCRVFIT, Protein Engineering Networks of Centres of Excellence v.2.1.1, http://www.bionmr.ualberta.ca/bds/software/xcrvfit/index.html.
50. Mercier, P., Spyracopoulos, L., and Sykes, B. D. (2001) Structure, dynamics, and thermodynamics of the structural domain of troponin C in complex with the regulatory peptide 1−40 of troponin I, *Biochemistry 40*, 10063−10077.
51. Blumenschein, T. M., Stone, D. B., Fletterick, R. J., Mendelson, R. A., and Sykes, B. D. (2005) Calcium-dependent changes in the flexibility of the regulatory domain of troponin C in the troponin complex, *J. Biol. Chem. 280*, 21924−21932.
52. Tripet, B., De Crescenzo, G., Grothe, S., O'Connor-McCourt, M., and Hodges, R. (2002) Kinetic analysis of the interactions between troponin C and the C-terminal troponin I regulatory region and validation of a new peptide delivery/capture system used for surface plasmon resonance, *J. Mol. Biol. 323*, 345.
53. Cachia, P. J., Sykes, B. D., and Hodges, R. S. (1983) Calcium-dependent inhibitory region of troponin: a proton nuclear magnetic resonance study on the interaction between troponin C and the synthetic peptide N^{α}-acetyl[FPhe^{106}]TnI-(104−115) amide, *Biochemistry 22*, 4145−4152.

BI051580L